4. C. M. Foran, B. N. Peterson, W. H. Benson, *Toxicol. Sci.* **68**, 389 (2002).
5. C. DeRosa, P. Richter, H. Pohl, D. E. Jones, *J. Toxicol. Environ. Health B Crit. Rev.* **1**, 3 (1998).
6. V. K. Rakyan *et al.*, *Proc. Natl. Acad. Sci. U.S.A.* **100**, 2538 (2003).
7. P. Hajkova *et al.*, *Mech. Dev.* **117**, 15 (2002).
8. G. Durcova-Hills, J. Ainscough, A. McLaren, *Differentiation* **68**, 220 (2001).
9. W. Reik, J. Walter, *Nat. Rev. Genet.* **2**, 21 (2001).
10. A. Jost, S. Magre, R. Agelopoulou, *Hum. Genet.* **58**, 59 (1981).
11. M. Buehr, S. Gu, A. McLaren, *Development* **117**, 273 (1993).
12. G. Majdic, M. R. Millar, P. T. Saunders, *J. Endocrinol.* **147**, 285 (1995).
13. H. O. Goyal *et al.*, *Anat. Rec.* **249**, 54 (1997).
14. W. R. Kelce, E. Monosson, M. P. Gamcsik, S. C. Laws, L. E. Gray Jr., *Toxicol. Appl. Pharmacol.* **126**, 276 (1994).
15. A. M. Cummings, *Crit. Rev. Toxicol.* **27**, 367 (1997).
16. K. W. Gaido *et al.*, *Endocrinology* **140**, 5746 (1999).
17. W. R. Kelce, C. R. Lambright, L. E. Gray Jr., K. P. Roberts, *Toxicol. Appl. Pharmacol.* **142**, 192 (1997).
18. J. S. Fisher, *Reproduction* **127**, 305 (2004).
19. R. E. Chapin *et al.*, *Fundam. Appl. Toxicol.* **40**, 138 (1997).
20. A. S. Cupp *et al.*, *J. Androl.* **24**, 736 (2003).
21. M. Uzumcu, H. Suzuki, M. K. Skinner, *Reprod. Toxicol.* **18**, 765 (2004).
22. B. S. Shi, Z. N. Cai, J. Yang, Y. N. Yu, *Mutat. Res.* **556**, 1 (2004).
23. H. Dong *et al.*, *Biochemistry* **43**, 15922 (2004).
24. A. Tokumura, *J. Cell. Biochem.* **92**, 869 (2004).

25. We acknowledge the technical contributions of I. Sadler-Riggleman, S. Rekow, and B. Johnston and the assistance of H. Suzuki with the methylation PCR procedure. This research was supported in part by a grant to M.K.S. from the U.S. Environmental Protection Agency's Science to Achieve Results (STAR) program involving endocrine disruptors.

Supporting Online Material
www.sciencemag.org/cgi/content/full/308/5727/1466/DC1
Materials and Methods
Figs. S1 to S3
References and Notes

2 December 2004; accepted 22 March 2005
10.1126/science.1108190

Kinesin and Dynein Move a Peroxisome in Vivo: A Tug-of-War or Coordinated Movement?

Comert Kural,[1] Hwajin Kim,[3] Sheyum Syed,[2] Gohta Goshima,[4] Vladimir I. Gelfand,[3]*† Paul R. Selvin[1,2]‡

We used fluorescence imaging with one nanometer accuracy (FIONA) to analyze organelle movement by conventional kinesin and cytoplasmic dynein in a cell. We located a green fluorescence protein (GFP)–tagged peroxisome in cultured *Drosophila* S2 cells to within 1.5 nanometers in 1.1 milliseconds, a 400-fold improvement in temporal resolution, sufficient to determine the average step size to be ~8 nanometers for both dynein and kinesin. Furthermore, we found that dynein and kinesin do not work against each other in vivo during peroxisome transport. Rather, multiple kinesins or multiple dyneins work together, producing up to 10 times the in vitro speed.

Conventional kinesin (kinesin-1) and cytoplasmic dynein are microtubule-dependent molecular motors responsible for organelle trafficking and cell division. The long-distance organelle transport within a cell occurs bidirectionally along the microtubule tracks. Plus (+) end directed kinesins carry the cargo to the cell periphery whereas minus (−) end directed dyneins bring the cargo back.

In vitro studies using optical traps (*1*) and single-molecule fluorescence imaging (*2*) have provided insight into how the microtubule motors work. Kinesin is a highly processive motor that can take hundreds of 8-nm steps, with a load of up to 6 pN, before detaching from the microtubule (*3*). Optical trap and in vitro motility studies have shown that a dynein-dynactin complex is also processive (*4*) and that dynein has an 8-nm step size under a load of up to 1.1 pN (*5*).

These studies, however, do not address how kinesin and dynein cooperate to achieve intracellular bidirectional transport. Do they move a cargo by engaging in a "tug-of-war," or is there a switch that turns off one or both of the motors? Do multiple motors of the same polarity act together or cooperatively (*6*–*8*)? Answering these questions requires observing the cargo molecules in vivo with high temporal and spatial resolution. In particular, the spatiotemporal resolution must be faster than the typical rate of moving at the physiological adenosine 5′-triphosphate (ATP) concentration.

We used fluorescence imaging with one nanometer accuracy (FIONA) (*2*, *9*) inside a live cell to track GFP-labeled peroxisomes being carried by microtubule motors with 1.5-nm accuracy and 1-ms time resolution, thereby allowing in vivo ATP concentrations. We used cultured *Drosophila* S2 cells that constitutively express enhanced green fluorescence protein (EGFP) with a peroxisome-targeting signal (*10*). Fluorescence images of peroxisomes, excited with total internal epifluorescence microscopy and labeled with numerous EGFP molecules, can be fit to a Gaussian function and then well-localized (Fig. 1). Figure 1 shows a cell in a bright-field image (treated as described below), a fluorescence image of the EGFP-peroxisomes, and a 1-ms point-spread-function of one peroxisome, which shows localization to 1.5 nm.

Most organelles use both microtubule motors and myosins for intracellular movement (*11*). To analyze the work of microtubule motors in the absence of myosin effects, we treated cells with 5 μM cytochalasin D, a drug that caps barbed ends of actin filaments, resulting in the disappearance of long filaments and therefore inhibition of actomyosin-dependent movement. Normal S2 cells plated on a substrate coated with concanavalin A have a discoid shape (*12*). Upon the loss of the actin filament network, S2 cells grow thin processes that are filled with microtubules (Fig. 1), but have no F-actin cables detectable by fluorescent phalloidin staining (*13*). We analyzed the polarity of microtubules in these processes using cells expressing EGFP-tagged EB1 (*12*). EB1 is a protein that specifically binds to (+) ends of growing microtubules (*14*). We found that in thin processes (diameter ≤ 1 μm), more than 90% of microtubules have (+) ends pointing away from the cell body (fig. S1). In contrast, in processes with a diameter >1 μm, only about 60% of microtubules have their (+) ends pointing away from the cell body, presumably due to a buckling of the microtubules inside the process. Consequently, only those peroxisomes moving in processes with a diameter <1 μm were analyzed (fig. S1).

Our measurements were performed at 10°C, and although low temperatures are known to favor microtubule depolymerization, immunofluorescent staining with antibody to tubulin demonstrated that the incubation at 10°C had no effect on the density or distribution of microtubules (fig. S2). We also determined the effect of microtubule lattice movements on peroxisome motion by performing fluorescence recovery after photo-

[1]Biophysics Center, [2]Physics Department, [3]Department of Cell and Structural Biology, University of Illinois, Urbana, IL 61801, USA. [4]Department of Cellular and Molecular Pharmacology, University of California, San Francisco, CA 94107, USA.

*Present address: Department of Cell and Molecular Biology, Feinberg School of Medicine, Northwestern University, Chicago, IL 60611, USA.
†To whom correspondence should be addressed. Department of Cell and Molecular Biology, Northwestern University School of Medicine, 303 East Chicago Avenue, Ward 11-080, Chicago, IL 60611–3008, USA. E-mail: vgelfand@northwestern.edu
‡To whom correspondence should be addressed. Loomis Lab of Physics, 1110 West Green Street, University of Illinois, Urbana, IL 61801, USA. E-mail: selvin@uiuc.edu

bleaching experiments on processes containing GFP-tubulin–based microtubules. The fluorescence recovery was longer than 1 s, indicating that microtubule lattice movements occur much more slowly than do kinesin- and dynein-driven organelle movements (fig. S4).

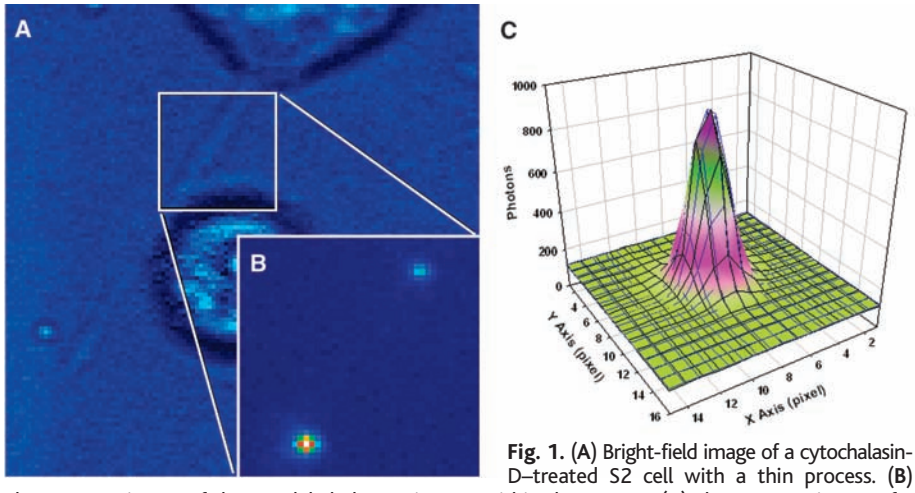

Fig. 1. (**A**) Bright-field image of a cytochalasin-D–treated S2 cell with a thin process. (**B**) Fluorescence image of the GFP-labeled peroxisomes within the process. (**C**) Fluorescence image of a peroxisome can be fit to a two-dimensional Gaussian (correlation coefficient $r^2 = 0.992$), enabling the center to be determined to 1.5 nm within 1.1 ms.

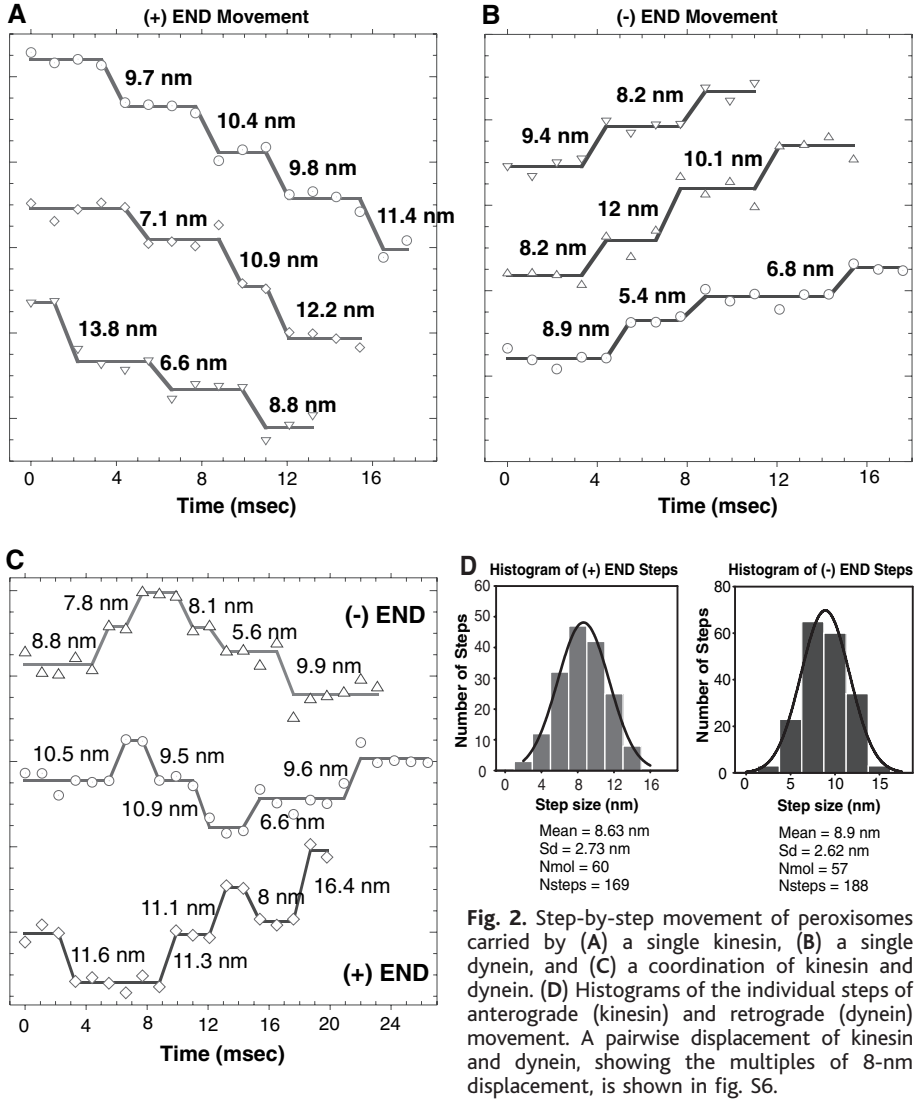

Fig. 2. Step-by-step movement of peroxisomes carried by (**A**) a single kinesin, (**B**) a single dynein, and (**C**) a coordination of kinesin and dynein. (**D**) Histograms of the individual steps of anterograde (kinesin) and retrograde (dynein) movement. A pairwise displacement of kinesin and dynein, showing the multiples of 8-nm displacement, is shown in fig. S6.

Drosophila S2 cells are highly sensitive to protein inhibition by RNA interference (RNAi) (*12*). We used RNAi to find which motors move peroxisomes along microtubules. We tested conventional kinesin (kinesin-1), three members of kinesin-2 family (Klp68D, Klp64D, and CG17461), three members of kinesin-3 family (Klp53D, Klp98A, and Klp38B), and ncd (a member of kinesin-14 or C-terminal kinesin family), as well as cytoplasmic dynein. We did not test depolymerizing kinesins, mitotic kinesins, and kinesins, which are not expressed above background level in S2 cells, as shown by microarray analysis (*15*). RNAi analysis showed that organelle transport was inhibited by RNAi only against kinesin-1 and dynein heavy chain, indicating that only these motors are responsible for movement (fig. S3).

FIONA localization showed that peroxisomes can move in a step-by-step manner in both anterograde (kinesin) and retrograde (dynein) directions (Fig. 2, A to C). With 169 motor steps, the average step size in the kinesin direction was 8.6 ± 2.7 nm (mean ± SD) (Fig. 3A), and the average speed was 1.5 ± 0.6 μm/s. In the dynein direction, 188 steps yielded an average step size of 8.9 ± 2.6 nm (Fig. 3B) and an average speed of 1.7 ± 0.9 μm/s. The step-size results are in agreement with in vitro kinesin and dynein assays (*3*, *5*), which yielded about 8 nm/step. The average speed for dynein (at a saturating ATP concentration) is within a factor of 2: 1.7 μm/s, as determined here, versus 0.7 μm/s (*4*) or 1.2 μm/s (*16*). It is within a factor of 2 of the calculated speed at the maximal rate of in vitro ATP hydrolysis by dynein [120 s^{-1} (*17*)], assuming one hydrolyzed ATP molecule per 8 nm/step (120 steps/s × 8 nm/step = 0.96 μm/s). Finally, the in vitro rate for kinesin is 1.0 μm/s (*4*), compared with 1.5 μm/s determined here.

Previous optical trap experiments on kinesin show that the bead-motor linkage behaves like an entropic spring (*3*). Consequently, if motors of opposite directions were operating simultaneously, then any compliance in the motor stalks would cause a degradation of step sizes, moving in either direction, as one motor took a step while its competitor was also bound to a microtubule (fig. S5). We found step sizes to be constant, implying that there is no "tug-of-war" between motors. It appears that motors are somehow regulated, being turned on or off in such a way that they are not simultaneously dragging the peroxisome. A distribution of the displacement driven by kinesins and dynein, showing 8-nm steps or multiples thereof, indicates no degenerated steps by opposite motors (fig. S6).

Figure 3, A and B, show a distribution of speeds for a peroxisome moving in the (+) or (−) directions. The graphs are highly spiked, at intervals corresponding to ≈1.2 μm/s, extending to ~12 μm/s. This implies that the spikes correspond to up to 11 kinesins

moving without appreciable hindrance from dynein (Fig. 3A), or up to 11 dyneins moving without much hindrance from kinesin (Fig. 3B). These distinct spikes in speed distribution occur when multiple kinesins and multiple dyneins hydrolyze ATP simultaneously in a stochastic manner, because reducing the cytoplasmic ATP concentration by an ATP-uncoupler FCCP (*p*-trifluoromethoxy carbonyl cyanide phenyl hydrazone) terminates the fast (>5 μm/sec) organelle transport (*13*).

In vitro kinesin assays do not show such high velocities; velocities of microtubules gliding on a kinesin-coated surface are independent of motor densities with 1 to 1000 kinesins/μm^2, yielding speeds just above 0.5 μm/s (*18*). In contrast, gliding assays done in more viscous media suggest that at higher loads, the velocity increases at higher motor densities (*19*), suggesting that kinesins can operate together. Other in vivo studies show similar fast organelle transport. Ashkin *et al*. have found that mitochondria carried on microtubules can move as fast as 15 μm/s (*20*). Endosomes in cells can be moved by dynein with speeds as fast as 4 μm/s, faster than the in vitro dynein speed (*21*). Maximum vesicle velocities in neurons are reported to be 3.5 to 5 μm/s, higher than can be achieved by a single microtubule-dependent motor (*22*–*25*).

Figure 4 shows traces of individual peroxisome movement, which demonstrate that the peroxisomes move at rates greater than the in vitro single-motor rate. Figure 4A shows one peroxisome moved by dynein at an average rate of 1.0 μm/s; kinesin then takes over for two steps, and then dynein takes over again, moving the peroxisome about two times as fast as the previous (−) end run (2.2 μm/s), still in a stepwise manner. Figure 4B shows a peroxisome moved by multiple (perhaps 11) kinesins, then by a few dyneins (perhaps two), then by kinesins (perhaps two), then by multiple dyneins. Figure 4C shows the movement of peroxisome to the (−) end at various speeds >150 ms. This clearly shows the ability of a peroxisome to be moved by several motors—up to 11 dyneins and 11 kinesins—without any apparent inhibition by the opposite motility partner.

The nature of the coordination between kinesin and dynein is unclear. One possibility is that a small molecule alternatively turns off kinesin and dynein, although it would have to react very quickly to account for a transition time of less than a millisecond between motors. Another possibility is that kinesin and dynein pull against one another until the stronger one "wins," which would cause the weaker one to uncouple quickly and therefore not creating any load. A third possibility is that the density and/or flexibility due to the lipid/membrane linkage of motor proteins on the peroxisomes are such that two motors of the opposite polarity cannot simultaneously bind to the microtubule. In either case, there must be a mechanism to allow the peroxisomes to move by multiple motors much faster than by independent, uncoupled, kinesins and dyneins.

Our results show that both kinesin and dynein move with 8-nm steps, transporting an organelle in vivo. Faster movements occur with the same step size but with greater rapidity. For the peroxisomes, in vivo, up to 11 kinesins or dyneins apparently can work in concert, driving the cargo much faster than seen in vitro.

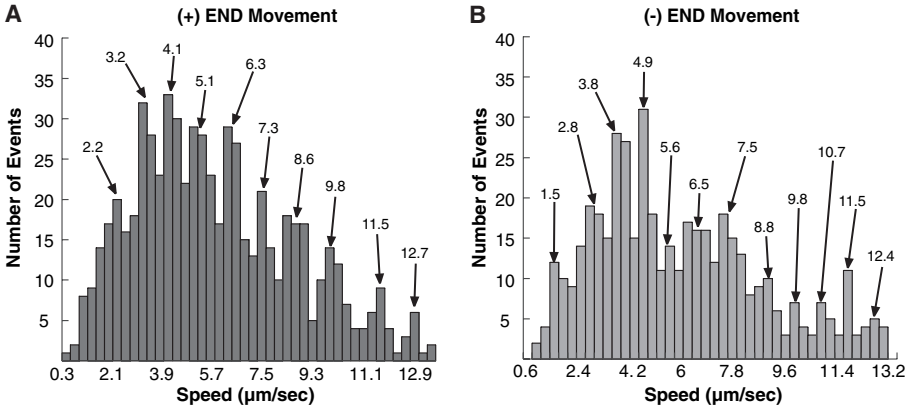

Fig. 3. (**A** and **B**) Stepping characteristics toward the (+) end (kinesin) and (−) end (dynein). Both graphs show multiple spikes, apparently corresponding to multiple kinesins [toward the (+) end] or dyneins [toward the (−) end] operating without load from the other motors. Both dynein and kinesin move rapidly (up to 12 μm/s), which is not seen in in vitro experiments. An event >20 nm was counted as a contiguous run (Fig. 4), independent of run length. The runs in the kinesin (+ end) and in the dynein (− end) directions were counted separately.

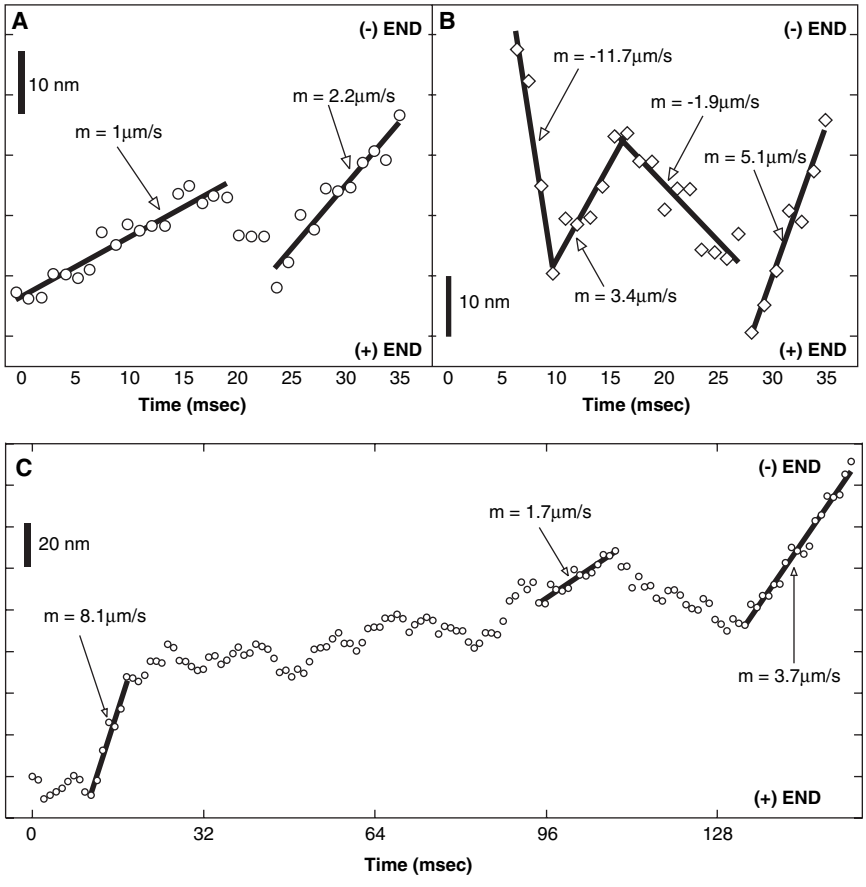

Fig. 4. Constant step size but variable speeds. (**A**) A peroxisome takes three steps driven by dynein, then two steps by kinesin, then about four steps by two dyneins, based on their average rate of stepping. (**B**) A peroxisome moved by about 11 kinesins, then two dyneins, then (one or) two kinesins, then three dyneins. (**C**) A peroxisome driven by dyneins at various speeds. (A), (B), and (C) are from different peroxisomes. "m" is the slope of the linear parts of the plot.

References and Notes

1. R. D. Vale, R. A. Milligan, *Science* **288**, 88 (2000).
2. A. Yildiz, M. Tomishige, R. D. Vale, P. R. Selvin, *Science* **303**, 676 (2004).
3. K. Svoboda, C. F. Schmidt, B. J. Schnapp, S. M. Block, *Nature* **365**, 721 (1993).
4. S. J. King, T. A. Schroer, *Nat. Cell Biol.* **2**, 20 (2000).
5. R. Mallik, B. C. Carter, S. A. Lex, S. J. King, S. P. Gross, *Nature* **427**, 649 (2004).
6. S. P. Gross, M. A. Welte, S. M. Block, E. F. Wieschaus, *J. Cell Biol.* **148**, 945 (2000).
7. R. Mallik, S. P. Gross, *Curr. Biol.* **14**, R971 (2004).
8. S. P. Gross *et al.*, *J. Cell Biol.* **156**, 855 (2002).
9. A. Yildiz *et al.*, *Science* **300**, 2061 (2003).
10. Materials and methods are available as supporting material on *Science* Online. For details of measurement, see (*9*). For microscopy, we used an Andor Model DV-860 BV, which is a back-illuminated camera that contains a 128 by 128 pixel sensor with 24 μm pixel size. A quarter chip is used to achieve 1 ms per frame. The incidence beam angle was tuned to get the best signal to noise. The cells were maintained at 10°C.
11. S. L. Rogers, V. I. Gelfand, *Curr. Opin. Cell Biol.* **12**, 57 (2000).
12. S. L. Rogers, G. C. Rogers, D. J. Sharp, R. D. Vale, *J. Cell Biol.* **158**, 873 (2002).
13. C. Kural *et al.*, data not shown.
14. Y. Ma, D. Shakiryanova, I. Vardya, S. V. Popov, *Curr. Biol.* **14**, 725 (2004).
15. G. Goshima, R. D. Vale, *J. Cell Biol.* **162**, 1003 (2003).
16. M. Nishiura *et al.*, *J. Biol. Chem.* **279**, 22799 (2004).
17. T. Kon, M. Nishiura, R. Ohkura, Y. Y. Toyoshima, K. Sutoh, *Biochemistry* **43**, 11266 (2004).
18. R. D. Vale, T. S. Reese, M. P. Sheetz, *Cell* **42**, 39 (1985).
19. A. J. Hunt, F. Gittes, J. Howard, *Biophys. J.* **67**, 766 (1994).
20. A. Ashkin, K. Schutze, J. M. Dziedzic, U. Euteneuer, M. Schliwa, *Nature* **348**, 346 (1990).
21. M. Lakadamyali, M. J. Rust, H. P. Babcock, X. Zhuang, *Proc. Natl. Acad. Sci. U.S.A.* **100**, 9280 (2003).
22. D. B. Hill, M. J. Plaza, K. Bonin, G. Holzwarth, *Eur. Biophys. J.* **33**, 623 (2004).
23. S. T. Brady, R. J. Lasek, R. D. Allen, *Science* **218**, 1129 (1982).
24. B. Grafstein, D. S. Forman, *Physiol. Rev.* **60**, 1167 (1980).
25. C. Kaether, P. Skehel, C. G. Dotti, *Mol. Biol. Cell* **11**, 1213 (2000).

26. We gratefully acknowledge R. Vale (University of California, San Francisco) and S. Rogers (University of North Carolina at Chapel Hill) for EGFP-EB1 and EGFP-tubulin cell lines. This work was supported by NIH grants AR44420 and GM 068625 (P.R.S.) and GM52111 (V.I.G.), an NSF grant (P.R.S.), and the U.S. Department of Energy, Division of Material Sciences (under award no. DEFG02-91ER45439), through the Frederick Seitz Materials Research Laboratory at the University of Illinois at Urbana-Champaign (P.R.S). P.R.S. also thanks J. Ackland, J. Stenehjem, and the other members of the Sharp Rehabilitation Center of San Diego for patient care, which made this science possible.

Supporting Online Material

www.sciencemag.org/cgi/content/full/1108408/DC1
Materials and Methods
Figs. S1 to S6
References

7 December 2004; accepted 30 March 2005
Published online 7 April 2005;
10.1126/science.1108408
Include this information when citing this paper.

Mechanism of Divergent Growth Factor Effects in Mesenchymal Stem Cell Differentiation

Irina Kratchmarova,[1]* Blagoy Blagoev,[1]* Mandana Haack-Sorensen,[2] Moustapha Kassem,[2] Matthias Mann[1]†

Closely related signals often lead to very different cellular outcomes. We found that the differentiation of human mesenchymal stem cells into bone-forming cells is stimulated by epidermal growth factor (EGF) but not platelet-derived growth factor (PDGF). We used mass spectrometry–based proteomics to comprehensively compare proteins that were tyrosine phosphorylated in response to EGF and PDGF and their associated partners. More than 90% of these signaling proteins were used by both ligands, whereas the phosphatidylinositol 3-kinase (PI3K) pathway was exclusively activated by PDGF, implicating it as a possible control point. Indeed, chemical inhibition of PI3K in PDGF-stimulated cells removed the differential effect of the two growth factors, bestowing full differentiation effect onto PDGF. Thus, quantitative proteomics can directly compare entire signaling networks and discover critical differences capable of changing cell fate.

Receptor tyrosine kinases (RTKs) regulate cellular processes ranging from cell growth and proliferation to survival and differentiation. After binding of their cognate ligands, these receptors undergo autophosphorylation on multiple tyrosine residues and become a platform for binding and consequent tyrosine phosphorylation of various signaling molecules, thus triggering multiple signaling cascades (*1*–*3*). To transmit the signal across the entire cell, various RTKs often activate universal signaling pathways. Nevertheless, distinct and even opposing biological effects of these receptors can arise.

Human mesenchymal stem cells (hMSC) are nonhematopoietic cells that reside within the bone marrow stroma. These cells are multipotent and serve as precursors for various mesoderm-type cells (*4*, *5*). Thus, hMSC have great clinical potential in tissue regeneration and engineering protocols (*6*). In cell culture, they can give rise to osteoblasts, adipocytes, and chondrocytes through processes largely controlled by various growth factors (*7*, *8*).

To study the effects of growth factors on hMSC, we first tested the effects of EGF, PDGF, fibroblast growth factor (FGF), and nerve growth factor (NGF) on cellular responses. Using immunoprecipitation and Western blotting with antibodies to phosphotyrosine, we observed that EGF and PDGF elicited the strongest responses (*9*) and that they induced phosphorylation of common and distinct subsets of proteins (Fig. 1A). Because one of the main characteristics of hMSC is their ability to differentiate to osteoblasts, we explored the possibility that these growth factors affect osteogenic conversion. The induction of the osteoblast differentiation pathway is indicated by increased alkaline phosphatase in the early stages (day 2 to 4), and in vitro mineralization is a marker for mature osteoblasts

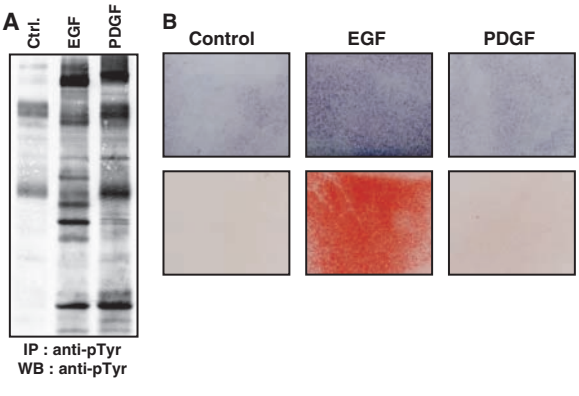

Fig. 1. Response of hMSC to EGF and PDGF stimulation. (**A**) Anti-phosphotyrosine (anti-pTyr) Western blotting (WB) of non-stimulated (Ctrl.) or EGF- or PDGF-stimulated hMSC, after immunoprecipitation (IP) with anti-pTyr. (**B**) Effects of EGF and PDGF on hMSC osteoblast differentiation. (Top) Alkaline phosphatase activity at day 3 of differentiation, visualized by in situ staining. (Bottom) Extracellular matrix in vitro mineralization after 9 days; staining with Alizarin Red S dye.

[1]Center for Experimental BioInformatics (CEBI), Department of Biochemistry and Molecular Biology, University of Southern Denmark, Campusvej 55, DK-5230 Odense M, Denmark. [2]Department of Endocrinology, Odense University Hospital, DK-5000 Odense C, Denmark.

*These authors contributed equally to this work.
†To whom correspondence should be addressed. E-mail: mann@bmb.sdu.dk